Ultrasonic bubbles in medicine: influence of the shell

Michiel Postema, Georg Schmitz

Session: Invited, ESS10

Version: November 21, 2006

Ultrasonic bubbles in medicine: influence of the shell

Michiel Postema[1], Georg Schmitz[1]

[1] Institute for Medical Engineering, Ruhr-Universität Bochum, Bochum, Germany.

corresponding author:

Michiel Postema, MSc, PhD, Institute for Medical Engineering, Department of Electrical Engineering and Information Technology, Ruhr-Universität Bochum, Building IC, 6/146, D-44780 Bochum, Germany;

tel: +49 234 32 27740; E-mail: michiel.postema@ruhr-uni-bochum.de

Running title: Medical bubble shell

Keywords: ultrasound contrast agent, shell disruption, fragmentation threshold, oscillation phase angle, shell elasticity, shell friction

Abstract

Ultrasound contrast agents consist of microscopically small bubbles encapsulated by an elastic shell. These microbubbles oscillate upon ultrasound insonification, and demonstrate highly nonlinear behavior, ameliorating their detectability. (Potential) medical applications involving the ultrasonic disruption of contrast agent microbubble shells include release-burst imaging, localized drug delivery, and noninvasive blood pressure measurement. To develop and enhance these techniques, predicting the cracking behavior of ultrasound-insonified encapsulated microbubbles has been of importance. In this paper, we explore microbubble behavior in an ultrasound field, with special attention to the influence of the bubble shell.

A bubble in a sound field can be considered a forced damped harmonic oscillator. For encapsulated microbubbles, the presence of a shell has to be taken into account. In models, an extra damping parameter and a shell stiffness parameter have been included, assuming that Hooke's Law holds for the bubble shell. At high acoustic amplitudes, disruptive phenomena have been observed, such as microbubble fragmentation and ultrasonic cracking. We analyzed the occurrence of ultrasound contrast agent fragmentation, by simulating the oscillating behavior of encapsulated microbubbles with various sizes in a harmonic acoustic field. Fragmentation occurs exclusively during the collapse phase and occurs if the kinetic energy of the collapsing microbubble is greater than the instantaneous bubble surface energy, provided that surface instabilities have grown big enough

to allow for break-up. From our simulations it follows that the Blake critical radius is not a good approximation for a fragmentation threshold.

We demonstrated how the phase angle differences between a damped radially oscillating bubble and an incident sound field depend on shell parameters.

1 Introduction

Ultrasonic imaging is an economic, reliable diagnostic technique. When taking into account the absolute hospital operating expenses [1], X-ray and ultrasound have approximately the same price per examination. Other imaging techniques are roughly three times as expensive, except for catheterization, which is twenty times as expensive [2]. However, X-ray is a less desirable imaging technique than ultrasound, due to the negative ionizing radiation effects. Therefore, novel ultrasound-based imaging techniques are being developed that may compete with other imaging techniques.

In clinical ultrasound, blood cells cannot be differentiated from surrounding tissue, due to the low acoustic impedance difference between blood cells and their surroundings. Resonant gas bubbles introduced in the blood stream are ideal markers, if rapid dissolution can be prevented. Ultrasound contrast agents consist of microscopically small bubbles encapsulated by an elastic shell. These microbubbles oscillate upon ultrasound insonification, and demonstrate highly nonlinear behavior, ameliorating their detectability. To enhance diagnostic ultrasound imaging techniques and to explore therapeutic applications, these medical microbubbles have been modeled.

For structures with radii r much less than the acoustic wavelength, such as red blood cells, the ultrasonic backscattering coefficient is [3]:

$$\eta(\omega) \propto k^4\, r^6 \left(\frac{\kappa_1 - \kappa_0}{\kappa_0} - \frac{\rho_1 - \rho_0}{\rho_0} \right)^2, \tag{1}$$

where k is the acoustic wave number, κ_1 is the compressibility of the scatterer, κ_0 is the compressibility of the surrounding medium, ρ_1 is the density of the scatterer, and ρ_0 is the density of the surrounding medium. Since the density and compressibility parameters of blood cells hardly differ from those of plasma, in the diagnostic ultrasonic frequency range, blood cells are poor scatterers. An ultrasound contrast agent has been added to the blood that helps to differentiate between blood and other tissue types, by providing additional and desirably characteristic backscatter [4]. Gas microbubbles are suitable contrast agents because of their high compressibility and low density compared to the surrounding medium. To prevent them from rapid dissolution, ultrasound contrast agents consist of air or slowly diffusing gas (*e.g.,* SF_6, C_3F_8) bubbles encapsulated by a

stabilizing elastic (*e.g.,* albumin, lipid) shell. With mean diameters below 6 μm, these bubbles are small enough to pass through capillaries. An overview of ultrasound contrast agents currently available and their applications has been given in [2].

(Potential) medical applications involving the disruption of microbubble shells include release-burst imaging [5], localized drug delivery [6, 7], and noninvasive blood pressure measurement [8]. To develop and enhance these techniques, predicting the cracking behavior of ultrasound-insonified encapsulated microbubbles has been of importance. In order to develop such predictive models, ultrasound contrast agents have been studied by measuring their acoustic response [9, 10], by (high-speed) photography during insonification [11, 12], and by atomic force microscopy [13].

In this paper, we explore microbubble behavior in an ultrasound field, with special attention to the influence of the bubble shell.

2 Theory

2.1 Linear, radially symmetric behavior

A bubble in a low-amplitude sound field can be considered a forced damped harmonic oscillator [14]:

$$m\,\ddot{x} + \beta\,\dot{x} + s\,x = F(\omega t), \tag{2}$$

where m is the mass of the bubble-liquid system [15], x the bubble excursion, β the mechanical resistance, s the stiffness of the system, and $F(\omega t)$ the driving force with a angular frequency ω. This system can be rewritten substituting the angular resonance frequency

$$\omega_0 = \sqrt{\frac{s}{m}} \tag{3}$$

and a dimensionless damping parameter

$$\delta = \frac{\beta}{m\,\omega}\,. \tag{4}$$

The damping of the pulsation is determined by the acoustic radiation, the heat conduction, and the liquid viscosity [16]. In [14], F. Ronald Young elegantly demonstrated that a solution of equation (2) has a phase angle difference $\alpha + \pi$ with the incident field, where

$$\alpha = \arctan\left(\frac{\left(\frac{\omega}{\omega_0}\right)\delta}{1 - \left(\frac{\omega}{\omega_0}\right)^2}\right). \tag{5}$$

For encapsulated microbubbles, the presence of a shell has to be taken into account, by adding an extra damping parameter:

$$\delta_{\mathrm{s}} = \frac{S_{\mathrm{f}}}{m\,\omega}\,, \tag{6}$$

where S_{f} is the shell friction [17]. Also, shell stiffness parameters χ, S_{sh} have been added, assuming that Hooke's Law holds for the bubble shell [16]:

$$\chi = \frac{S_{\mathrm{sh}}}{8\pi} = \frac{\mathbf{E}\,\epsilon}{1-\nu}\,, \tag{7}$$

where $\mathbf{E}$ is Young's modulus, ϵ is the shell thickness, and ν is the Poisson ratio. The shell stiffness can be assessed from atomic force microscopy [13], estimated from optical observations of radius–time curves [11, 12] or derived from acoustical data using the relation [18]:

$$\omega_{\mathrm{s}}^2 \approx \omega_0^2 + \frac{2\chi}{r_0^3\,\rho}\,, \tag{8}$$

where ω_{s} is the angular resonance frequency of the encapsulated microbubble, ω_0 is the angular resonance frequency of a free (unencapsulated) microbubble of the same size, r_0 is the equilibrium radius of the bubble, and ρ is the liquid density.

2.2 Nonlinear, radially symmetric behavior

When the ultrasonic driving pressure is sufficiently high, the nonlinear microbubble response results in harmonic dispersion, which not only produces harmonics with frequencies that are integer multiples of ω (superharmonics) but also subharmonics with frequencies less than ω of the form $m\omega/n$, where $\{m, n\} \in \mathbb{N}$ [19]. The nonlinear oscillating behavior of spherically symmetric single bubbles has been described by models based on the Rayleigh-Plesset equation [14, 19]. De Jong added shell stiffness and friction terms and showed that the shells surrounding the ultrasound contrast agent Albunex® could be modeled as an elastic solid [17]. This model proved to be useful for thin lipid shells, as well [20, 2]. Church derived a general theoretical model for the case of a bubble whose surface is occupied by molecules which behave collectively as a continuous, damped, elastic solid [21]. This model has been modified many times to predict the dynamic behavior of ultrasound contrast agents [11, 22, 23, 24, 25, 26, 27]. These models take into account the surface tension, the (in)compressibility of the liquid, the viscosity of the shell, and the fact that the gas in the bubble is compressed and expanded according to the gas law. Most of the modified models are referred to as zero-thickness encapsulation models, since these assume the bubble shell to be very thin and describe only the dynamics of the outer bubble radius. Recently, Sarkar et al. presented viscous and viscoelastic rheological models of the bubble shell [28]. Doinikov and Dayton generalized Church's theory, by allowing for the translation motion of the bubble and radiation losses due to the

compressibility of the surrounding liquid. Also, models accounting for large-amplitude oscillations have become of interest [29].

At low acoustic amplitudes (mechanical index MI<0.1), microbubbles pulsate linearly. At high amplitudes (MI>0.6), their elongated expansion phase is followed by a violent collapse. During the collapse phase, when the kinetic energy of the bubble surpasses its surface energy, a bubble may fragment into a number of smaller bubbles. Fragmentation has been exclusively observed with contrast agents with thin, elastic shells. Fragmentation is the dominant disruption mechanism for these bubbles [12].

During the initial part of the collapse the acceleration, $\ddot{r}$ is negative. This sign changes as the gas inside the bubble begins to be compressed, and the rebound begins [30]. Provided that surface instabilities have grown big enough to allow for break-up, microbubble fragmentation has been expected and observed close to this moment, when $\ddot{r} = 0$ [31]. This has been confirmed by means of high-speed photography [12, 32]. The occurrence of fragmentation has been associated with inertial cavitation [31, 10]. Thresholds have been proposed, above which a bubble behaves like an inertial cavity [14]:

$$\frac{r_{\mathrm{B}}}{r_0} = c\,, \tag{9}$$

where $r_{\mathrm{B}} = \max(r(t))|_{\mathrm{B}}$ is the so-called Blake critical radius and c is the threshold constant which has been approximated by $c \approx 2$. The number of fragments N into which a microbubble breaks up, is related to the dominant spherical harmonic oscillation mode n by [30, 12]:

$$N \approx n^3\,. \tag{10}$$

Mode 2 oscillations have been observed with lipid-encapsulated microbubbles, leading to fragmentation into 8 newly formed microbubbles [12].

Let us consider a single spherically symmetric microbubble with an inner radius r_{i} and an outer radius r, a shell density ρ_{s}, negligible translation, in an infinite fluid with density ρ. The kinetic energy of such a microbubble can be approximated by [27]:

$$E_{\mathrm{k}} \approx 2\pi\,\rho\,r^3\,\dot{r}^2 \; + 2\pi\,\rho_{\mathrm{s}}\,r_{\mathrm{i}}^3\,\dot{r}_{\mathrm{i}}^2\left(1 - \frac{r_{\mathrm{i}}}{r}\right). \tag{11}$$

Knowing that, for microbubbles with monolayer lipid shells, $\dfrac{r_{\mathrm{i}}}{r} < 0.01$ and $\rho_{\mathrm{s}} = 1.15 \times 10^3\ \mathrm{kg\,m^{-3}}$, and for blood, $\rho = 1.05 \times 10^3\ \mathrm{kg\,m^{-3}}$ [26], equation (11) can be simplified to [30]:

$$E_{\mathrm{k}} \approx 2\pi\,\rho\,r^3\,\dot{r}^2\,. \tag{12}$$

The surface free energy E_{s} of a single encapsulated bubble is given by [27]:

$$E_{\mathrm{s}} = 4\pi\,r_{\mathrm{i}}^2\,\mu_1 + 4\pi\,r^2\,\mu_2\,, \tag{13}$$

where μ_1 and μ_2 denote the surface tension coefficients for the inner and outer interface, respectively. For our microbubbles with monolayer lipid shells, we consider a single interface model, using the effective surface tension μ [27]:

$$\mu = \mu_1 + \mu_2 \,. \tag{14}$$

After fragmentation, the resulting microbubble fragments contain more surface free energy $\sum_i E_{\mathrm{f},i}$ than the single bubble prior to fragmentation:

$$\sum_{i=1}^{N} E_{\mathrm{f},i} \approx \tfrac{4}{3}\pi\, r_{\mathrm{f}}^2\, \mu\, N \approx \tfrac{4}{3}\pi\, r^2\, \mu\, N^{\frac{1}{3}} = N^{\frac{1}{3}}\, E_{\mathrm{s}}\,, \tag{15}$$

where r_{f} is the mean fragment radius. Neglecting the elastic energy of the shell, the internal energy of the gas core, it can be assumed that fragmentation will only occur if [32]:

$$E_{\mathrm{k}} > \left(\sum_{i=1}^{N} E_{\mathrm{f},i} - E_{\mathrm{s}} \right). \tag{16}$$

2.3 Nonlinear, radially asymmetric behavior

Although asymmetric shape bubble oscillations have been observed [12, 33], within our size range, spherical harmonic modes higher than 2 can be neglected [12]. For asymmetric shape oscillations, more complicated models are being developed.

At high acoustic amplitudes (MI>0.6), disruptive phenomena have been observed, such as microbubble fragmentation and ultrasonic cracking [12]. Again, assuming that Hooke's Law holds for the bubble shell, the critical stress at which a shell ruptures is:

$$\sigma_{\mathrm{c}} = \mathbf{E}\, \epsilon_{\mathrm{c}}\,, \tag{17}$$

where $\mathbf{E}$ is Young's modulus and ϵ_{c} is the critical lateral shell deformation. For example, the critical stress of the thick-shelled contrast agent Quantison$^{\mathrm{TM}}$ is $\sigma_{\mathrm{c}} \geq 80$ kPa [34], and thus $\epsilon_{\mathrm{c}} \geq 0.4$. Generally, for biomaterials, $\epsilon_{\mathrm{c}} < 0.5$ [35].

For microbubbles of radius with a thick, stiff shell, such as Quantison$^{\mathrm{TM}}$, $\max(r(t)) \ll r_0$. The stability of such a shell under low-amplitude insonification has been modeled in [36]. Thick-shelled bubbles have demonstrated gas release during a high-amplitude ultrasonic cycle [37, 12]. The increased pressure difference between inside and outside of the bubble during the expansion phase of the wave causes the shell to be stretched across the critical deformation, resulting into its mechanical cracking. The released bubble has an oscillation amplitude much higher than an encapsulated bubble of the same size [12]. Quantitative studies on this so-called sonic cracking have been presented in [37, 12].

On the contrary, microbubbles with a thin, highly elastic monolayer lipid shell, like SonoVue^{TM} and other Bracco agents, have been observed to expand to more than ten-fold their initial surface areas during rarefaction. The shell behaves like an elastic membrane that ruptures under relatively small strain [38, 39]. By the time of maximal expansion, therefore, the shell has ruptured, leaving newly formed clean free interfaces.

3 Methods

We simulated the oscillating behavior of encapsulated microbubbles with various sizes in a harmonic acoustic field:

$$p_{\mathrm{a}}(t) = p^{-} \sin \omega t \,, \tag{18}$$

where p^{-} denotes the peak negative acoustic pressure. The modified Rayleigh-Plesset equation as stated in [20] was solved using MATLAB® (The MathWorks, Inc., Natick, MA) programs. We used the same parameters as in [20], noting that the vapor pressure should be p_{v}=2.33 kPa. Shell parameters $\chi = 1.1$ kg s^{-2} and S_{f}=0.27×10^{-6} kg s^{-1} were included [40]. We did not approximate $\delta(r(t))$ by a time-averaged damping coefficient. Thermal damping was neglected [16]. The acoustic amplitudes modeled correspond to MI≪2 (well within the clinical diagnostic range). We focused on simulated driving frequencies ranging from 0.5 to 5.0 MHz.

For microbubbles with radii 0.2< r_0 <12.0 μm, the critical acoustic pressures p_{c} were computed, above which eq. (16) holds. For comparison with the Blake critical radius, the maximal microbubble radii $\max r(r_0, p_{\mathrm{c}})$ were computed using the modified Rayleigh-Plesset equation, and divided by the initial radii r_0.

The phase angle differences $\phi = \alpha + \pi$ between p_{a} and r were computed for free and encapsulated microbubbles under low-amplitude insonification. Radii were chosen 0.1< r_0 <8.0 μm. Known shell stiffness and friction parameters of two ultrasound contrast agents were included. For the resonance frequencies of free gas microbubbles, we included a surface tension term [14]. Again, thermal damping was neglected [16]. Since $|r(t)| \ll r_0$, here, we approximated $\delta(r(t))$ by a time-averaged damping coefficient $\delta(r_0)$.

4 Results and discussion

It has been previously demonstrated, with the aid of high-speed photography, that the oscillation, translation, coalescence, and jetting behavior of a microbubble with a thin, lipid shell is comparable to that of a free microbubble, as opposed to the behavior of thick-shelled bubbles [12].

Figure 1 demonstrates the simulated oscillation behavior of a lipid-encapsulated microbubble, insonified at

3 MHz ultrasound with $p^- = 1.2$ MPa. The relatively slow expansion is followed by a rapid collapse. Close to the collapse, the kinetic energy of the microbubble becomes higher than the surface energy. This is the oscillation phase where microbubble break-up has been expected and observed.

Figure 2, left column, shows the critical pressures above which equation (16) holds, for free gas microbubbles (frame a) and for a lipid-shelled microbubbles (frame c). In frame a, the critical pressure is minimal around resonance size ($r_0 \approx 6.5\,\mu$m). Since the resonance frequency of the contrast microbubbles is increased, owing to stiffness of the shell, the minimum in frame c has been shifted to a radius greater than 8 μm. Furthermore, local minima can be appreciated at harmonic resonance sizes. At relatively low acoustic pressures, only microbubbles with sizes close to resonance will fragment. The corresponding maximal expansion radii at the critical pressures normalized by the initial radii are demonstrated in frames b and d, respectively. In contradiction to the assumption that the Blake critical radius is a good approximation for a fragmentation threshold, our simulations show $r_{\rm B}/r_0 \ll 2$ for most microbubbles.

Figure 3 shows three curves of the phase angle differences ϕ between a damped radially oscillating bubble and an incident 4 MHz sound field, as a function of r_0. The curves have been computed for a free microbubble, a SonoVue$^{\rm TM}$ contrast microbubble, and an Albunex® contrast microbubble. With increasing shell stiffness, the bubble resonance size increases. At resonance, the bubble oscillates $\phi = \frac{3}{2}\pi$ rad out of phase with the sound field. For bubble greater than resonance, the phase angle difference approaches 2π rad, so that the bubble oscillates in phase with the sound field. Below resonance size, ϕ has a minimum value still greater than π, and approaches $\frac{3}{2}\pi$ for r_0 much smaller than resonance size. Since the damping due to the liquid viscosity $\delta_{\rm v} \propto r^{-2}$, ϕ approaches $\frac{3}{2}\pi$ for a free bubble radius $r_0 < 1$ μm. The approach to $\frac{3}{2}\pi$ below the minimum of ϕ is stronger with the contrast bubbles, because $\delta_{\rm s} \propto r^{-3}$. As the damping becomes greater, the phase transition around resonance becomes less abrupt, as Figure 3 demonstrates.

The high-speed photographs in Figure 4 illustrate the shift in ϕ. The central bubble (bubble 1) has an equilibrium radius of 4.3 μm, whereas the upper left bubble (bubble 2) has an equilibrium radius of 1.7 μm. Maximal expansion of bubble 2 can be seen in frame 5, where $\max(r_2(t)) = 2.1$ μm. Maximal expansion of bubble 1, however, is seen in frame 7, where $\max(r_1(t)) = 13$ μm. Hence, bubble 1 oscillates $\frac{2}{3}\pi$ rad out of phase with respect to bubble 2.

5 Conclusions

Microbubble fragmentation occurs exclusively during the collapse phase and will only occur if the kinetic energy of the collapsing microbubble is greater than the instantaneous bubble surface energy. Our simulations demonstrate fragmentation thresholds for bubbles of different sizes. It follows that the Blake critical radius is not a good approximation for a fragmentation threshold.

We demonstrated how the phase angle differences between a damped radially oscillating bubble and an incident sound field depend on shell parameters.

References

[1] Canadian Institute for Health Information, Medical imaging in Canada (2004).

[2] M. Postema, G. Schmitz, Bubble dynamics involved in ultrasonic imaging, Expert Rev. Mol. Diagn. 6 (3) (2006) 493–502.

[3] G. Schmitz, Ultrasound in medical diagnosis, in: R. Pike, P. Sabatier (Eds.) Scattering: scattering and inverse scattering in pure and applied science, Academic Press, London, 2002, pp. 162–174.

[4] E. G. Schutt, D. H. Klein, R. M. Mattrey, J. G. Riess, Injectable microbubbles as contrast agents for diagnostic ultrasound imaging: the key role of perfluorochemicals, Angew. Chem. Int. Ed. 42 (2003) 3218–3235.

[5] P. J. A. Frinking, E. I. Céspedes, J. Kirkhorn, H. G. Torp, N. de Jong, A new ultrasound contrast imaging approach based on the combination of multiple imaging pulses and a separate release burst, IEEE Trans. Ultrason., Ferroelect., Freq. Contr. 48 (3) (2001) 643–651.

[6] R. Bekeredjian, P. A. Grayburn, R. V. Shohet, Use of ultrasound contrast agents for gene or drug delivery in cardiovascular medicine, J. Am. Coll. Cardiol. 45 (3) (2005) 329–335.

[7] R. Bekeredjian, H. A. Katus, H. F. Kuecherer, Therapeutic use of ultrasound targeted microbubble destruction: a review of non-cardiac applications, Ultraschall in Med. 27 (2) (2006) 134–140.

[8] A. Bouakaz, P. J. A. Frinking, N. de Jong, N. Bom, Noninvasive measurement of the hydrostatic pressure in a fluid-filled cavity based on the disappearance time of micrometer-sized free gas bubbles, Ultrasound Med. Biol. 25 (9) (1999) 1407–1415.

[9] J. Guan, T. J. Matula, M. Averkiou, Imaging the destruction of individual ultrasound contrast microbubbles with diagnostic ultrasound, Acoust. Res. Lett. Online 5 (4) (2004) 165–169.

[10] A. Y. Ammi, R. O. Cleveland, J. Mamou, G. I. Wang, S. L. Bridal, W. D. O'Brien Jr., Ultrasonic contrast agent shell rupture detected by inertial cavitation and rebound signals, IEEE Trans. Ultrason., Ferroelect., Freq. Contr. 53 (1) (2006) 126–136.

[11] K. E. Morgan, J. S. Allen, P. A. Dayton, J. E. Chomas, A. L. Klibanov, K. W. Ferrara, Experimental and theoretical evaluation of microbubble behavior: Effect of transmitted phase and bubble size, IEEE Trans. Ultrason., Ferroelect., Freq. Contr. 47 (6) (2000) 1494–1509.

[12] M. A. B. Postema, Medical Bubbles, Universal Press, Veenendaal, 2004.

[13] V. Sboros, E. Glynos, S. D. Pye, C. M. Moran, M. Butler, J. Ross, R. Short, W. N. McDicken, V. Koutsos, Nanointerrogation of ultrasonic contrast agent microbubbles using atomic force microscopy, Ultrasound Med. Biol. 32 (4) (2006) 579–585.

[14] F. R. Young, Cavitation, McGraw-Hill, Maidenhead, 1989.

[15] H. Medwin, Counting bubbles acoustically: a review, Ultrasonics 15 (1977) 7–13.

[16] N. de Jong, L. Hoff, T. Skotland, N. Bom, Absorption and scatter of encapsulated gas filled microspheres: theoretical considerations and some measurements, Ultrasonics 30 (2) (1992) 95–103.

[17] N. de Jong, R. Cornet, C. T. Lancée, Higher harmonics of vibrating gas-filled microspheres. Part one: simulations, Ultrasonics 32 (6) (1994) 447–453.

[18] N. de Jong, A. Bouakaz, P. Frinking, Basic acoustic properties of microbubbles, Echocardiography 19 (3) (2002) 229–240.

[19] C. E. Brennen, Cavitation and bubble dynamics, Oxford University Press, Inc, New York, 1995.

[20] M. Postema, N. de Jong, G. Schmitz, The physics of nanoshelled microbubbles, Biomed. Tech. 50 (S1) (2005) 748–749.

[21] C. C. Church, The effects of an elastic solid surface layer on the radial pulsations of gas bubbles, J. Acoust. Soc. Am. 97 (3) (1995) 1510–1521.

[22] J. S. Allen, D. J. May, K. W. Ferrara, Dynamics of therapeutic ultrasound contrast agents, Ultrasound Med. Biol. 28 (6) (2002) 805–816.

[23] E. Stride, N. Saffari, Theoretical and experimental investigation of the behaviour of ultrasound contrast agent particles in whole blood, Ultrasound Med. Biol. 30 (11) (2004) 1495–1509.

[24] E. Stride, N. Saffari, Investigating the significance of multiple scattering in ultrasound contrast agent particle populations, IEEE Trans. Ultrason., Ferroelect., Freq. Contr. 52 (12) (2005) 2332–2345.

[25] H. Zheng, A. Barker, R. Shandas, Predicting backscatter characteristics from micron- and submicron-scale ultrasound contrast agents using a size-integration technique, IEEE Trans. Ultrason., Ferroelect., Freq. Contr. 53 (3) (2006) 639–644.

[26] H. Zheng, O. Mukdadi, R. Shandas, Theoretical predicitions of harmonic generation from submicron ultrasound contrast agents for nonlinear biomedical ultrasound imaging, Phys. Med. Biol. 51 (2006) 557–573.

[27] A. A. Doinikov, P. A. Dayton, Spatio-temporal dynamics of an encapsulated gas bubble in an ultrasound field, J. Acoust. Soc. Am. 120 (2) (2006) 661–669.

[28] K. Sarkar, W. T. Shi, D. Chatterjee, F. Forsberg, Characterization of ultrasound contrast microbubbles using in vitro experiments and viscous and viscoelastic interface models for encapsulation, J. Acoust. Soc. Am. 118 (1) (2005) 539–550.

[29] P. Marmottant, S. van der Meer, M. Emmer, M. Versluis, N. de Jong, S. Hilgenfeldt, D. Lohse, A model for large amplitude oscillations of coated bubbles acounting for buckling and rupture, J. Acoust. Soc. Am. 118 (6) (2005) 3499–3505.

[30] C. E. Brennen, Fission of collapsing cavitation bubbles, J. Fluid Mech. 472 (2002) 153–166.

[31] J. E. Chomas, P. Dayton, D. May, K. Ferrara, Threshold of fragmentation for ultrasonic contrast, J. Biomed. Opt. 6 (2) (2001) 141–150.

[32] M. Postema, G. Schmitz, Ultrasonic fragmentation of microbubbles: a theoretical approach of the flash in flash-echo, Proc. IEEE Eng. Med. Biol. Soc. (2005) 4023–4026.

[33] M. Versluis, S. M. van der Meer, D. Lohse, P. Palanchon, D. Goertz, C. T. Chin, N. de Jong, Microbubble surface modes, Proc. IEEE Ultrason. Symp. 1 (2004) 207–209.

[34] P. J. A. Frinking, N. de Jong, Acoustic modeling of shell-encapsulated gas bubbles, Ultrasound Med. Biol. 24 (4) (1998) 523–533.

[35] H. Abé, K. Hayashi, M. Sato, Data Book on Mechanical Properties of Living Cells, Tissues, and Organs, Springer-Verlag, Tokyo, 1996.

[36] B. Krasovitski, E. Kimmel, Stability of an encapsulated bubbles shell, Ultrasonics 44 (2006) 216–220.

[37] S. H. Bloch, M. Wan, P. A. Dayton, K. W. Ferrara, Optical observation of lipid- and polymer-shelled ultrasound microbubble contrast agents, Appl. Phys. Lett. 84 (4) (2004) 631–633.

[38] Z. Zhou, B. Joós, Mechanisms of membrane rupture: from cracks to pores, Phys. Rev. B 56 (6) (1997) 2997–3009.

[39] M. A. Borden, D. E. Kruse, C. F. Caskey, S. Zhao, P. A. Dayton, K. W. Ferrara, Influence of lipid shell physicochemical properties on ultrasound-induced microbubble destruction, IEEE Trans. Ultrason., Ferroelect., Freq. Contr. 52 (11) (2005) 1992–2002.

[40] J. M. Gorce, M. Arditi, M. Schneider, Influence of bubble size distribution on the echogenicity of ultrasound contrast agents: A study of SonoVue$^{\mathrm{TM}}$, Invest. Radiol. 35 (11) (2000) 661–671.

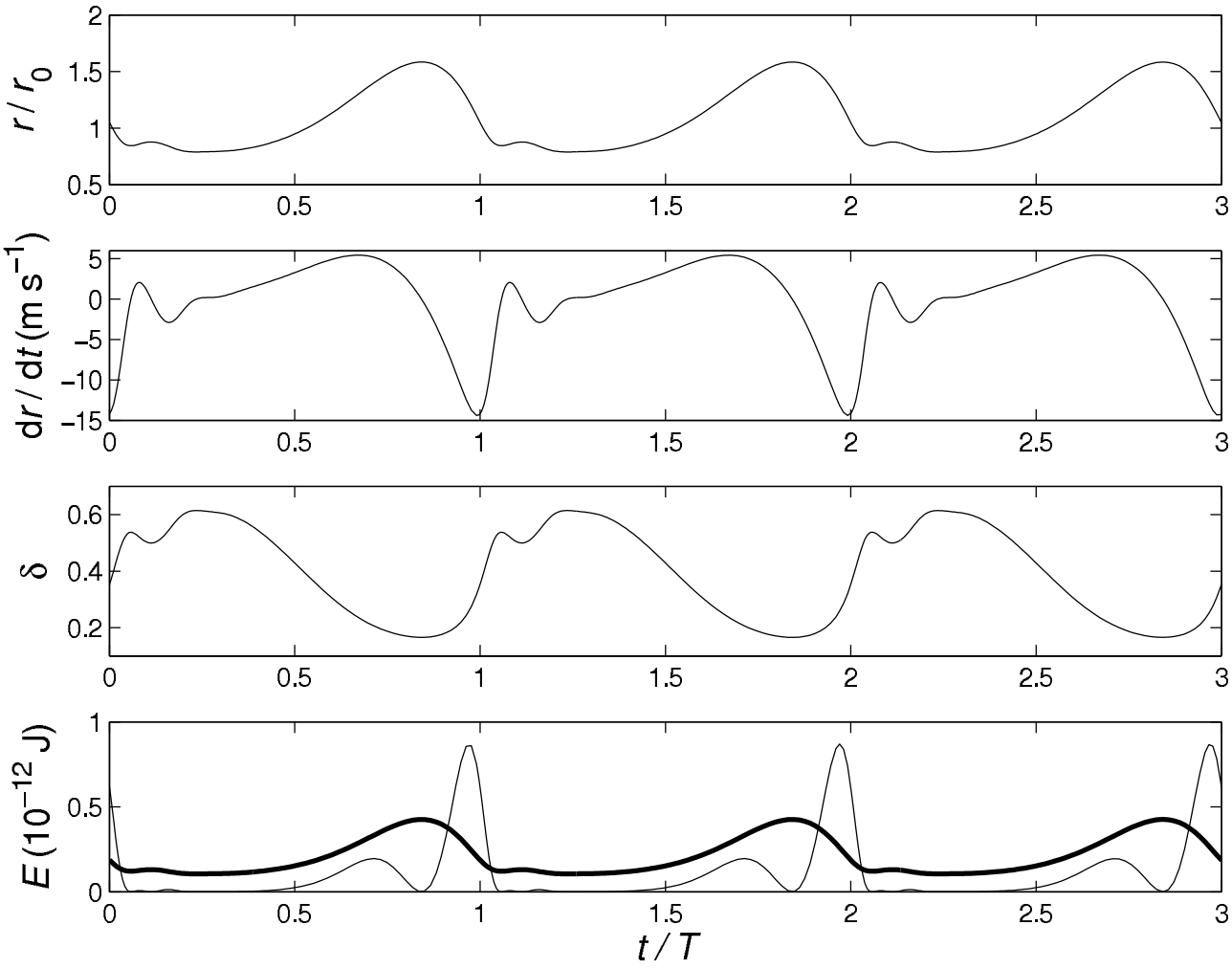

Figure 1: Simulation of the oscillation behavior of an encapsulated microbubble with an equilibrium radius $r_0 = 0.75$ μm and shell properties $\chi = 1.1$ kg s^{-2} and $S_\mathrm{f} = 0.27 \times 10^{-6}$ kg s^{-1} [40], during insonification at $f = 3.0$ MHz and $p^- = 1.2$ MPa, as a function of time t normalized by period T. The thin line in the lower frame is the kinetic energy of the bubble, whereas the bold line represents the right-hand side of equation (16).

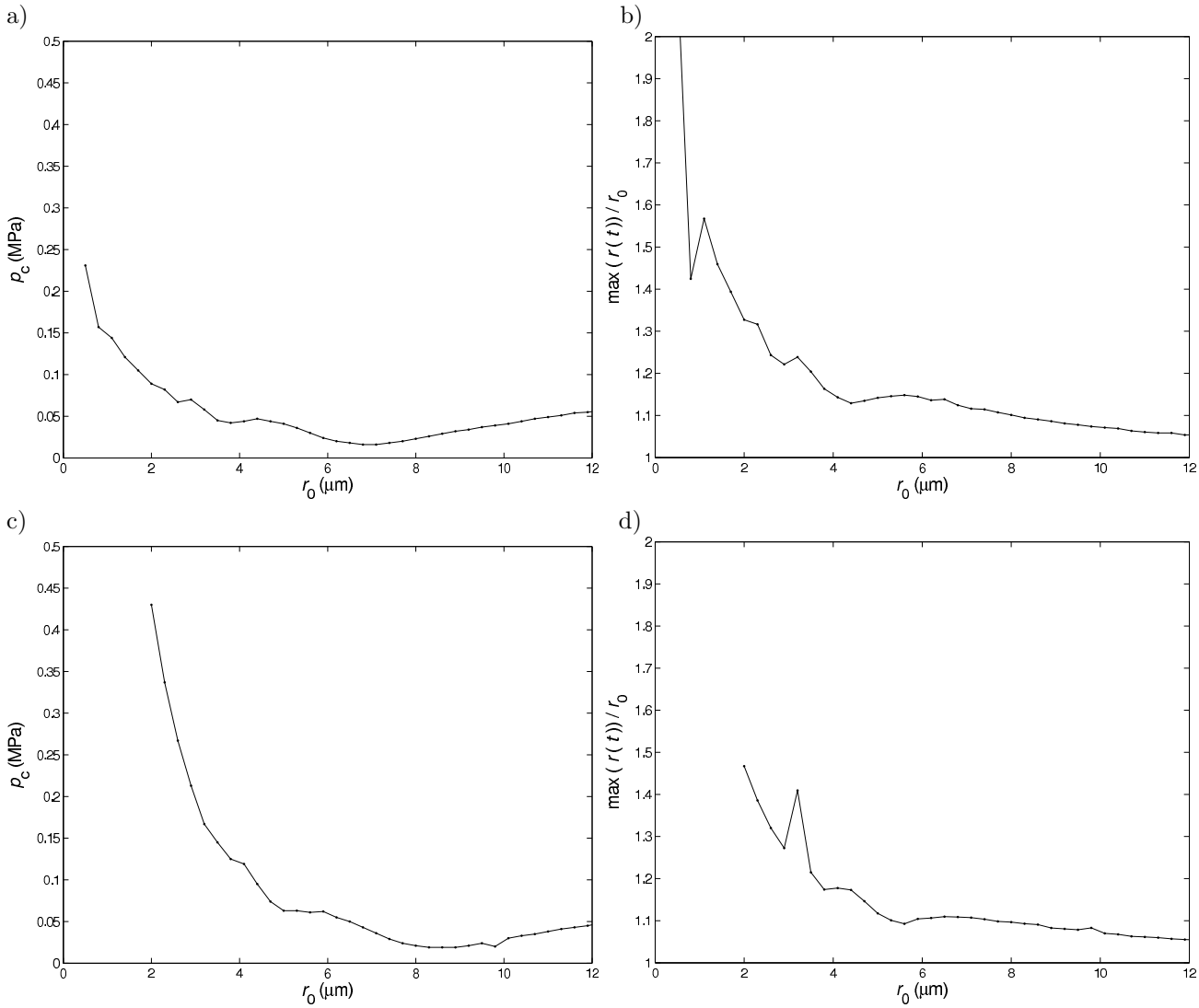

Figure 2: Critical pressure of 0.5 MHz ultrasound as a function of initial radius (a,c). Relative critical microbubble excursion at the critical pressure as a function of initial radius (b,d). The upper frames were computed for free gas microbubbles, the lower for lipid-shelled microbubbles.

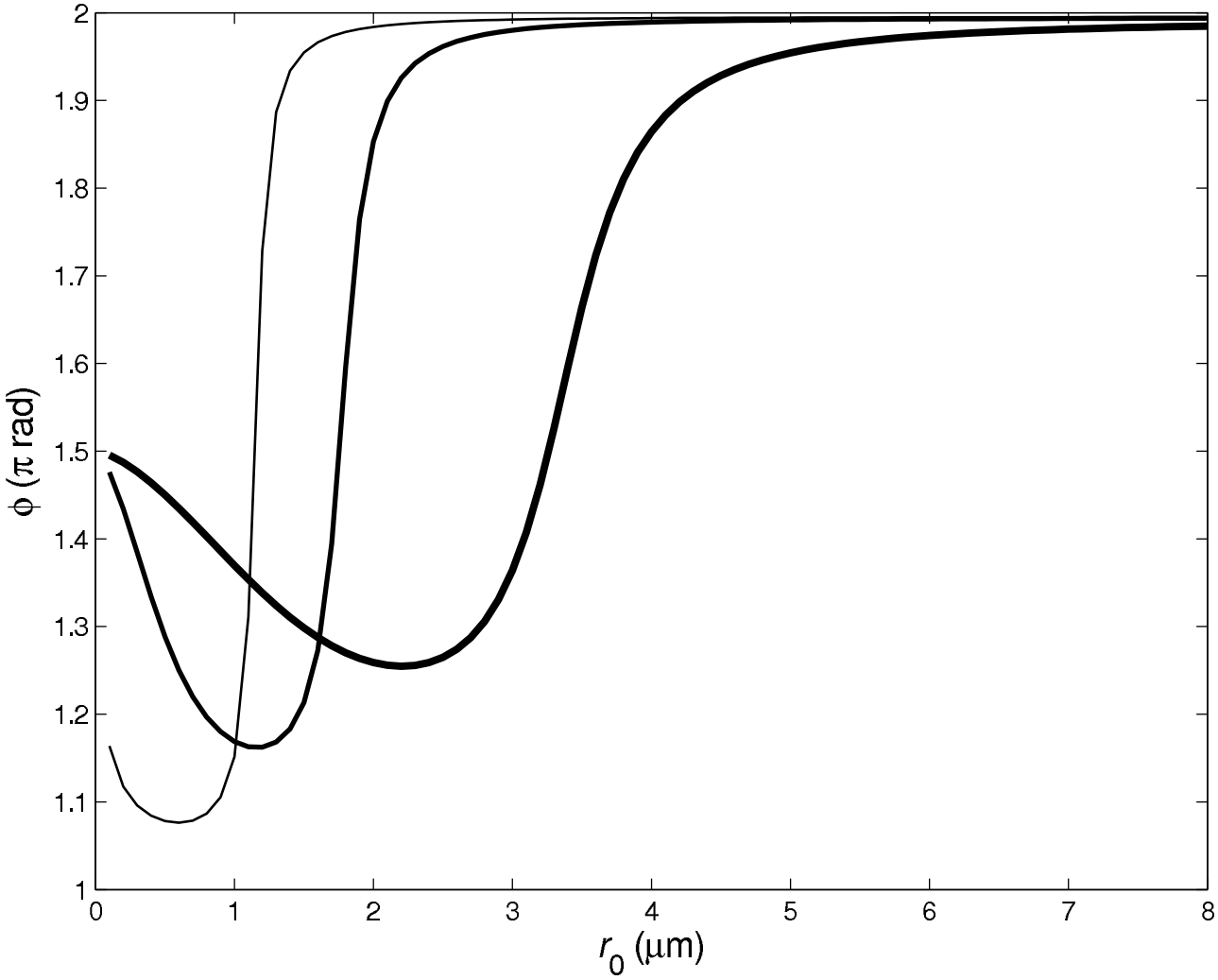

Figure 3: Phase angle difference ϕ between a damped radially oscillating bubble and an incident 4 MHz sound field, as a function of equilibrium radius r_0. The thin line represents a free bubble: $\chi = 0$ kg s^{-2}, $S_\mathrm{f} = 0$ kg s^{-1}; the bold line a SonoVue$^{\mathrm{TM}}$ microbubble: $\chi = 1.1$ kg s^{-2}, $S_\mathrm{f} = 0.27 \times 10^{-6}$ kg s^{-1} [40]; the fat line an Albunex® microbubble: $\chi = 10$ kg s^{-2}, $S_\mathrm{f} = 4 \times 10^{-6}$ kg s^{-1} [17].

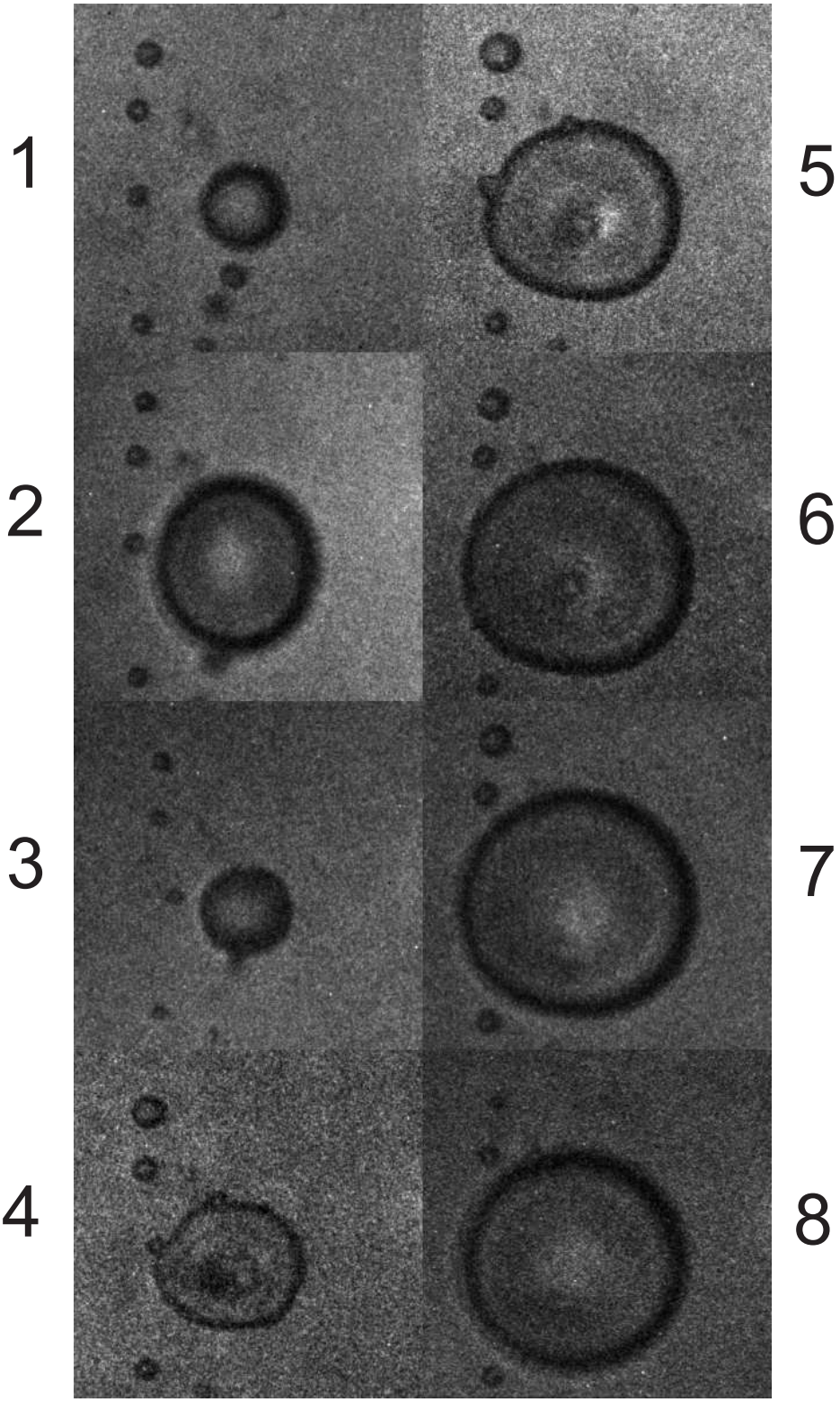

Figure 4: Sequence of high-speed photographs of BR14 contrast microbubbles (Bracco Research SA, Genève, Switzerland) insonified at 0.5 MHz. Frame 1 has been captured prior to ultrasound arrival. The other seven frames cover one full ultrasonic cycle, *i.e.* 2 μs. Each frame corresponds to a $40\times40\,\mu\mathrm{m}^2$ area. © 2005 Schiele & Schön GmbH. Reprinted with permission from [20].